Neutron Science

For over a decade, neutron scattering has served as a cornerstone of Taiwan's research into condensed matter physics and advanced materials. To ensure that Taiwanese researchers maintained access to world-class neutron facilities, the National Science and Technology Council (NSTC) spearheaded strategic international partnerships and oversaw the design and construction of **SIKA**, the Cold Neutron Triple-axis Spectrometer. Named after the Formosan sika deer, the instrument was officially commissioned at the Australian Nuclear Science and Technology Organisation (ANSTO) in 2015. On September 4, 2025, the NSRRC and ANSTO celebrated SIKA's 10th anniversary, marking a milestone in a collaboration that has achieved a 99% instrument availability rate, making **SIKA** the most stable facility of its kind in the Asia-Pacific region.

Together, synchrotron X-ray and neutron scattering provide a comprehensive and complementary toolkit for probing the heart of matter. Neutrons, with intrinsic spin and no charge, can precisely determine magnetic ordering and spin textures that are inaccessible to other techniques. By contrast, synchrotron X-rays offer exceptional brightness and energy tunability to resolve atomic arrangements and electronic structures with high precision. This dual-probe approach has been instrumental in several recent breakthroughs:

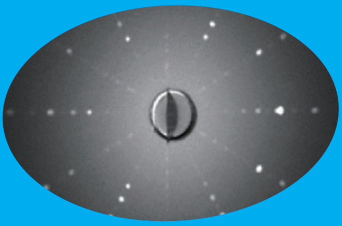

- **Quantum Spintronics**: Research using small-angle neutron scattering (SANS) on the **QUOKKA** instrument revealed that the Anomalous Hall Effect is driven by wild quantum spin fluctuations rather than static magnetism.

- **Thermoelectric Efficiency**: Using **SIKA**, researchers provided the first experimental observation of "phonon avoided-crossing." This interaction between acoustic phonons and rattling modes explains the material›s ultralow thermal conductivity, which is key to efficient energy conversion.

- **Ferroelectric Interfaces**: Neutron reflectometry on the **SPATZ** instrument allowed scientists to probe buried interfaces in thin films, identifying how interface engineering stabilizes the ferroelectric phase, which is crucial for next-generation electronic memory.

- **Multiferroics and Skyrmions**: High-intensity diffraction on **WOMBAT** helped determine complex spin structures, revealing how pressure can expand the stability of the skyrmion phase, and offering new pathways for high-density data storage.

Leveraging the Taiwan-Australia bilateral agreement, the scientific community has gained seamless access to both **SIKA** and a broader array of advanced instruments at ANSTO. This partnership has been instrumental in fostering academic excellence, as evidenced by numerous publications in top-tier journals. As a premier example of international cooperation, **SIKA** continues to enhance global visibility and provide a robust foundation for the long-term advancement of visionary materials science. (by Yu-Chun Chuang)

Direct Observation of Phonon Avoided-Crossing as the Origin of Ultralow Thermal Conductivity in β-Zn$_4$Sb$_3$

Momentum-resolved neutron spectra clearly reveal strong coupling between the acoustic phonon and the rattling mode, resulting in suppressed lattice thermal conductivity.

Thermoelectric (TE) materials are notable for directly converting waste heat into electricity without moving parts or chemical reactions.[1] The efficiency of a TE material is characterized by the dimensionless figure of merit, $zT = S^2\sigma\kappa^{-1}T$, where S is the Seebeck coefficient, σ is the electrical conductivity, and κ is the thermal conductivity. A higher zT indicates better conversion performance. Therefore, improving thermoelectric efficiency fundamentally requires increasing S and σ and/or reducing κ.

Among thermoelectric materials, zinc antimonides are the earliest and only Te-free compounds successfully used in thermoelectric generator development.[2] Within this family, p-type β-Zn$_4$Sb$_3$ has attracted particular attention due to its intrinsically high zT, achievable even without intentional alloying. β-Zn$_4$Sb$_3$ crystallizes in a rhombohedral structure (space group R$\bar{3}$c) and is widely recognized as a phonon-glass electron-crystal material.[3] Structural studies indicate extensive atomic disorder, with excess Zn atoms distributed across multiple interstitial sites. These highly mobile Zn interstitials, which can rapidly hop between available voids as predicted theoretically, are believed to be responsible for the remarkably low lattice thermal conductivity (κ_L) observed in β-Zn$_4$Sb$_3$.[4] Combined with a small bandgap (~0.8 eV) that allows for conductivity enhancement through dilute doping, β-Zn$_4$Sb$_3$ offers a tunable phonon–electron landscape for efficient TE energy conversion.

Chi-Hung Lee (Tunghai University), Hsin-Jay Wu (National Taiwan University), and their co-workers recently reported the first experimental observation of phonon avoided crossing in β-Zn$_4$Sb$_3$ using single-crystal inelastic neutron scattering at **SIKA**, establishing the microscopic origin of its glass-like lattice thermal conductivity (κ_l).[5] Structurally, Zn atoms occupy multiple defect and interstitial sites, producing strong dynamic disorder, while Sb forms a stable rhombohedral framework, with rattling Sb$_2$ units generating a flat phonon mode. Previous theoretical work proposed that rattlers may hybridize with acoustic phonons to form avoided crossings, a key mechanism underlying ultralow lattice thermal conductivity in host-guest materials such as skutterudites and clathrates. However, direct experimental evidence remains rare, as only single-crystal inelastic neutron scattering can resolve directional phonon dispersions.

The inelastic neutron scattering measurements on single-crystalline β-Zn$_4$Sb$_3$ unambiguously resolve a phonon avoided-crossing interaction as the central dynamical feature of this material. As shown in **Fig. 1(a)**, the longitudinal acoustic (LA) branch disperses linearly from Γ, as expected for a crystalline solid at small q, but its behavior deviates markedly near 6–8 meV. Instead of intersecting the low-lying rattling mode, the LA mode gradually flattens. This is a clear indication that its propagation is disrupted

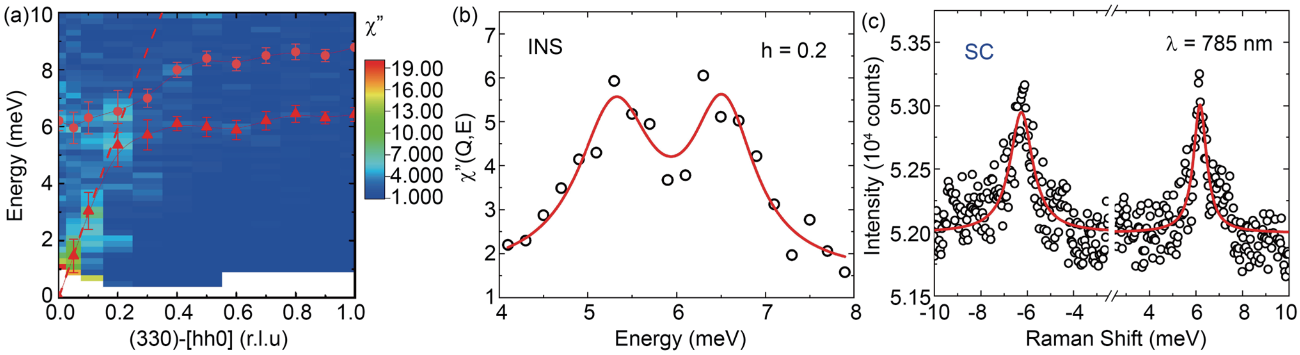

Fig. 1: (a) Longitudinal phonon dispersion of β-Zn$_4$Sb$_3$ at 300 K along [hh0]. The dashed line represents a sinusoidal function, and the color scale denotes the dynamic response according to the scattering intensities. Error bars correspond to the full width at half maximum extracted from Lorentzian peak fitting. (b) Constant-Q scan at (330) – [0.2 0.2 0], taken near the acoustic–rattling interaction region, revealing two well-resolved phonon peaks. (c) Room-temperature Raman spectrum of the single crystal excited with a 785 nm laser, confirming the low-lying rattling mode. Solid curves in (a) and (c) represent Lorentzian fits. [Reproduced from Ref. 5]

by another phonon mode. Meanwhile, the rattling mode does not pass through the LA mode but curves upward, deflected away rather than intersecting, resulting in a well-defined energy gap between the two branches. This mutual repulsion of phonon branches constitutes the avoided-crossing event.

The coupling becomes directly visible in the momentum-resolved neutron intensity. In the constant-Q cuts (**Fig. 1(b)**), instead of a single peak, two clear distinct peaks appear simultaneously at the same momentum transfer; this indicates the presence of two phonon branches in close energy proximity. These peaks remain well-separated rather than merging, showing that the modes do not cross but coexist as two resolvable excitations. The existence of this rattling mode is further verified by Raman spectroscopy, where distinct Stokes and anti-Stokes signals appear at 6.17(2) and −6.26(3) meV at room temperature (**Fig. 1(c)**). These symmetric peaks correspond to a rattling mode of ~6.2 meV (≈50 $\mathrm{cm^{-1}}$) at Γ, confirming the presence of a low-lying mode which participates in the avoided crossing observed in neutron scattering.

Overall, the neutron spectra reveal that acoustic phonons in β-$\mathrm{Zn_4Sb_3}$ are intercepted by a low-energy rattling mode and forced into an avoided-crossing state. Because acoustic branches are the primary heat carriers, their dispersion flattening leads to a pronounced reduction in group velocity, thus directly suppressing heat transport. Simultaneously, hybridization with the rattling mode strengthens anharmonic scattering and accelerates phonon decay. The observed linewidth yields an exceptionally short acoustic phonon lifetime of ~0.86 ps, markedly lower than that of conventional crystalline thermoelectrics, and also restricts lattice thermal transport. The reduction of phonon velocity and the ultrafast decay resulting from avoided crossing provides a microscopic mechanism for the intrinsically ultralow κ_L in β-$\mathrm{Zn_4Sb_3}$. (Reported by Chi-Hung Lee, Tunghai University)

This report features the work of Chi-Hung Lee, Hsin-Jay Wu and their co-workers published in Adv. Sci. ***12****, 2411498 (2025).*

ANSTO SIKA – Cold Neutron Triple-Axis Spectrometer

- Inelastic Neutron Scattering
- Materials Science, Condensed-matter Physics

References

1. G. S. Nolas, D. T. Morelli, T. M. Tritt, Annu. Rev. Mater. Res. **29**, 89 (1999).
2. T. Caillat, J. P. Fleurial, A. Borshchevsky, J. Phys. Chem. Solids **58**, 1119 (1997).
3. G. J. Snyder, M. Christensen, E. Nishibori, T. Caillat, B. B. Iversen, Nat. Mater. **3**, 458 (2004).
4. T. Zou, X. Qin, Y. Zhang, X. Li, Z. Zeng, D. Li, J. Zhang, H. Xin,W. Xie, A. Weidenkaff, Sci. Rep. **5**, 17803 (2015).
5. I-L. Jen, C.-Y. Lin, K.-K. Wang, C.-M. Wu, C.-H. Lee, H.-J. Wu, Adv. Sci. **12**, 2411498 (2025).

From Motionless to Mad Dance: Neutron Scattering Reveals the Hidden Driver of the Anomalous Hall Effect

Collinear spins with no static chirality still produce a giant anomalous Hall effect—driven purely by wild quantum spin fluctuations, revealed by neutron scattering. A revolutionary new mechanism for future spintronics.

In today's rapidly advancing technological landscape, the materials within our electronic devices are becoming as critical as the devices themselves. As we pursue faster computing, more efficient communication, and highly secure data storage, researchers are increasingly turning to quantum materials—systems in which electrons behave in unexpected ways. Leading this research is Pengcheng Dai's (Rice University, USA) team, whose studies continue to uncover new magnetic and electronic phenomena in complex materials. Their latest investigation of the kagome-lattice magnet $\mathrm{YbFe_6Ge_6}$, shown in **Fig. 1**, marks another significant advance, revealing how subtle quantum effects could one day transform the technologies that shape our lives.

Future electronics aim to control not only electric charge but also electron spin, a field known as spintronics, which promises faster, more efficient, and robust devices. A key phenomenon is the anomalous Hall effect (AHE), where a transverse voltage appears without an external magnetic field.[1]

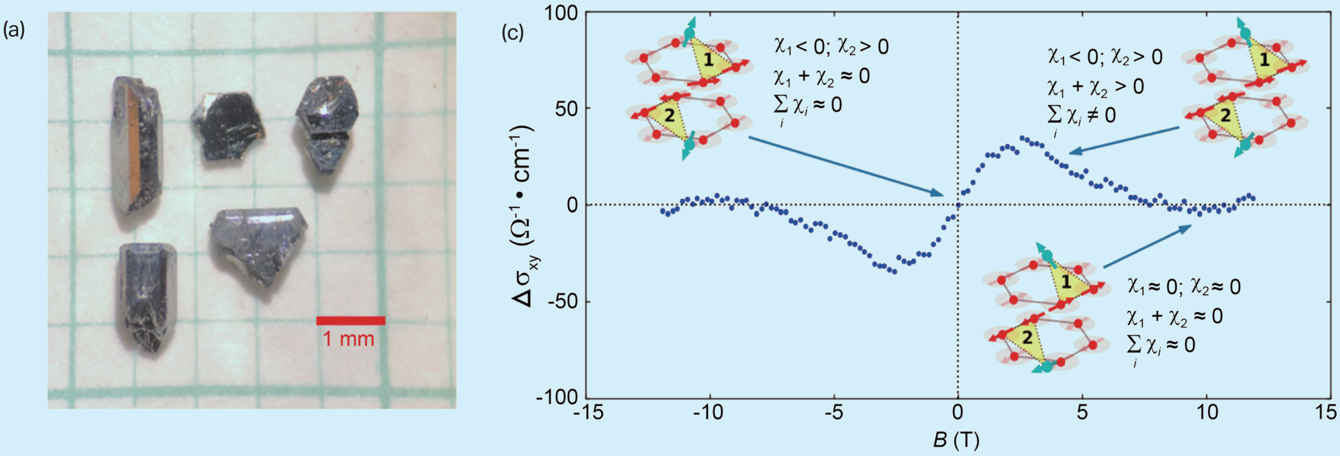

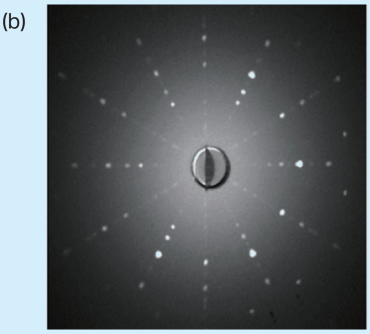

Fig. 1: (a) Typical $\mathrm{YbFe_6Ge_6}$ single crystals arranged on a millimeter grid. (b) X-ray Laue diffraction pattern measured on the (0, 0, L) surface. (c) Anomalous Hall conductivity $\Delta\sigma_{xy}$ at 10 K. The insets illustrate how the spin arrangements of Yb (cyan) and Fe (red) respond to different magnetic-field strengths, indicated by the blue arrows. The yellow triangles (labeled “1” and “2”) mark two representative Yb–Fe spin triads. Light red arrows depict the static magnetic configuration that develop below temperature of spin reorientation, while the light red circles outline the “easy plane” where the Fe spins prefer to align. For clarity, the spin-canting angles are intentionally exaggerated. [Reproduced from Ref. 2]

Dai’s team found that in $\mathrm{YbFe_6Ge_6}$, the AHE arises from dynamic spin fluctuations, not static spin patterns. Below 63 K, iron spins rotate into the kagome plane, triggering the AHE even though the spins remain aligned. Neutron scattering revealed these fluctuations are gapless, allowing brief local chirality that deflects electrons. Above 63 K, the gap suppresses fluctuations and the AHE disappears. This shows that the AHE can be driven by quantum spin motion rather than static magnetism.[2,3]

The neutron scattering experiments were conducted at several leading facilities, but one instrument was especially important: **QUOKKA**, the small-angle neutron scattering (SANS) instrument at the Australian Nuclear Science and Technology Organisation (ANSTO). SANS is highly sensitive to long-wavelength, low-momentum magnetic structures, making it well suited for detecting subtle field-induced features or nanoscale textures that may accompany the AHE.

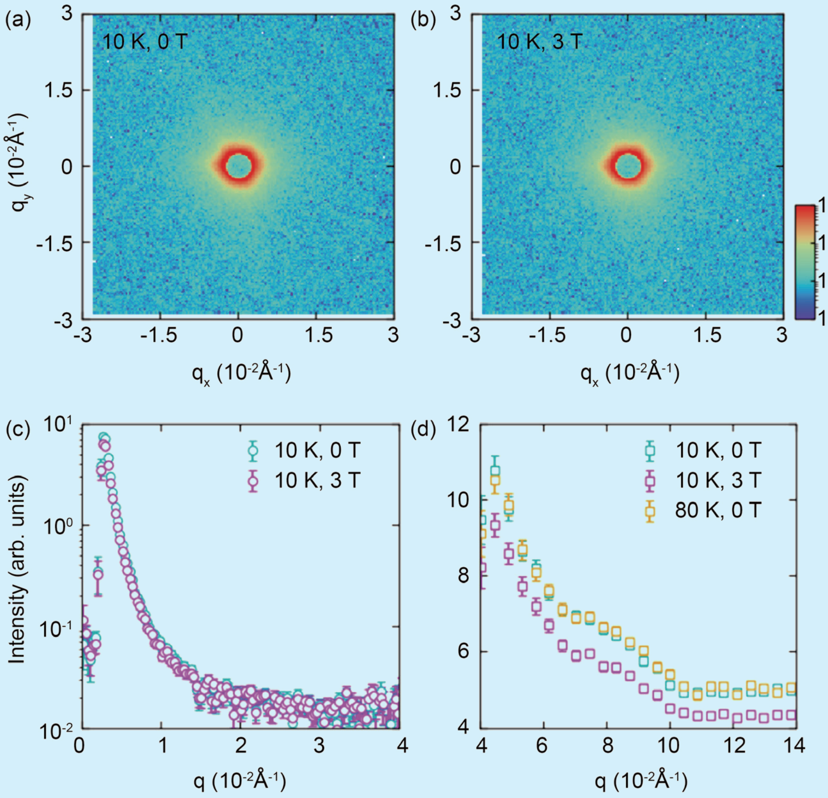

Fig. 2: (a,b) SANS patterns at 10 K, 0 T and 10 K, 3 T measured with the low-q setup. (c,d) Azimuthally averaged SANS intensities as a function of momentum transfer in the low-q and high-q setups, respectively. [Reproduced from Ref. 2]

The team used **QUOKKA** to search for such features when a magnetic field was applied in the material's plane. Importantly, they found no evidence of static magnetic textures, such as skyrmions or other chiral structures.[2] This absence was as significant as a positive detection because it ruled out conventional explanations[4] and strengthened the case that the observed AHE originates from dynamic, rather than static, magnetic behavior.

QUOKKA's ability to reveal what was not there helped clarify what was. By ruling out field-induced static chirality, the SANS measurements supported the team's theory: the AHE arises solely from fluctuating spins interacting with conduction electrons, with ytterbium ions subtly influencing spin orientation and enhancing fluctuations at low temperatures.

In summary, this research demonstrates how complex magnetic materials can exhibit unexpected quantum behaviors that may be useful for future technology. The work led by Dai shows that even materials with simple collinear antiferromagnetic structures can display rich electronic responses when their spins fluctuate appropriately. Neutron scattering, particularly using instruments like **QUOKKA**, was crucial in uncovering the hidden dynamics behind these effects. As scientists seek efficient, low-energy methods to manipulate electron spin, discoveries like this expand the possibilities and open new directions for quantum materials research. (Reported by Chun-Ming Wu)

This report features the work of Pengcheng Dai and his collaborators published in Phys. Rev. Lett. ***134****, 186501(2025).*

ANSTO QUOKKA – Small-angle Neutron Scattering

- SANS
- Condensed-matter Physics

References

1. N. Nagaosa, J. Sinova, S. Onoda, A. H. MacDonald, N. P. Ong, Rev. Mod. Phys. **82**, 1539 (2010).
2. W. Yao, S. Liu, H. Kikuchi, H. Ishikawa, Ø. S. Fjellvåg, D. W. Tam, F. Ye, D. L. Abernathy, G. D. A. Wood, D. Adroja, C.-M. Wu, C.-L. Huang, B. Gao, Y. Xie, Y. Gao, K. Rao, E. Morosan, K. Kindo, T. Masuda, K. Hashimoto, T. Shibauchi, P. Dai, Phys. Rev. Lett. **134**, 186501 (2025).
3. W. Wang, M. W. Daniels, Z. Liao, Y. Zhao, J. Wang, G. Koster, G. Rijnders, C.-Z. Chang, D. Xiao, W. Wu, Nat. Mater. **18**, 1054 (2019).
4. S. Nakatsuji, N. Kiyohara, T. Higo, Nature **527**, 212 (2015).

Ordered Spin Structures of Multiferroic and Skyrmion Compounds

Neutron scattering is a unique probe for spin correlations.

The neutron diffraction technique, developed in the 1930s, has become an indispensable tool for investigating complex behaviors in magnetic, multiferroic, and strongly correlated materials. Due to the neutron's intrinsic spin and charge neutrality, it interacts directly with magnetic moments, enabling precise determination of magnetic ordering, spin textures, and subtle structural distortions that often accompany electronic phase transitions. In multiferroics, where electric and magnetic orders coexist and frequently couple in intricate ways, neutron diffraction reveals the symmetry-breaking mechanisms that link lattice, charge, and spin degrees of freedom. In strongly correlated systems, neutron scattering uncovers collective excitations, long-range correlations, and hidden order parameters that conventional probes cannot detect. By providing sensitivity to both nuclear and magnetic structures, neutron diffraction offers a coherent, microscopic view of how competing interactions shape exotic ground states and emergent phenomena, making it a cornerstone technique in contemporary condensed matter physics.

For researchers in Taiwan, the Australian Centre for Neutron Scattering (ACNS) at Australian Nuclear Science and Technology Organisation (ANSTO) offers a unique opportunity. The Neutron Group of the NSRRC, based at ACNS, can assist Taiwan researchers in various ways. Hung-Duen Yang (National Sun Yat-sen University)

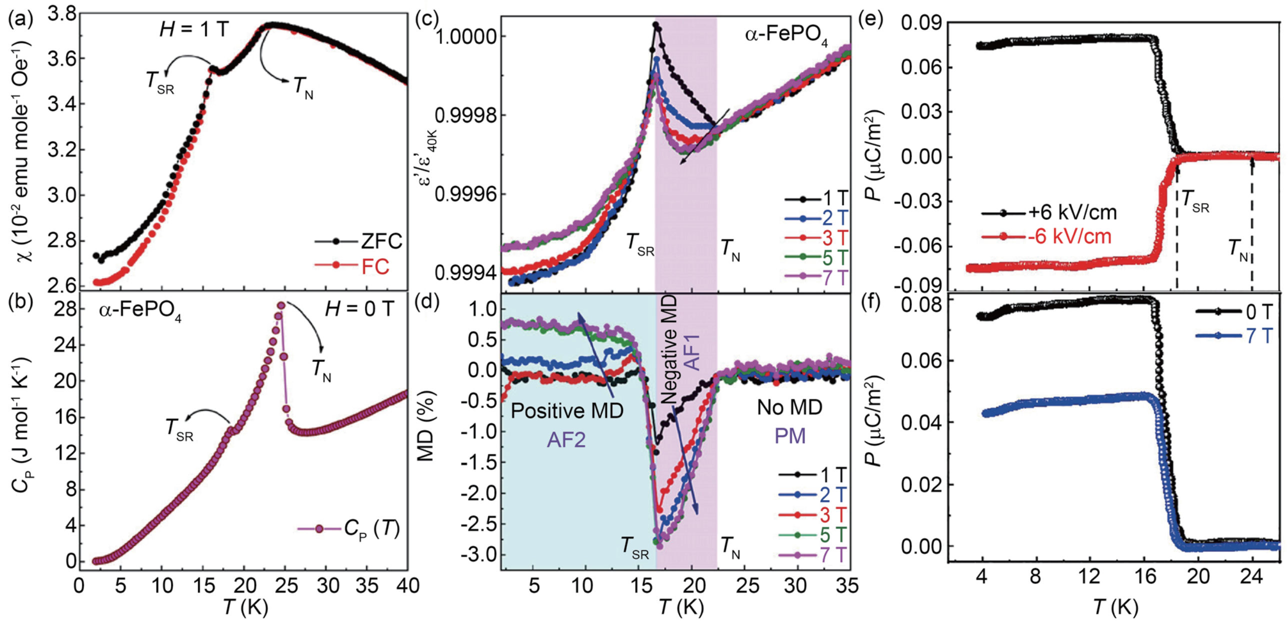

Fig. 1: (a) χ vs. T at $H = 1$ T (Zero field cool/Field cool) for α-FePO₄ showing the presence of two distinct magnetic transitions at T ≈ 25 K and T_{SR} ~ 17 K, which are further supported by (b) specific heat measurements at $H = 0$ T. (c) ε' vs. T curves under various H. (d) MD%, calculated from ε' vs. T, indicates a sign change in MD from negative to positive at the onset of T_{SR}. (e) Electric polarization (P), measured after cooling under different poling fields, is determined by integrating current (I) over time at $H = 0$ T. (f) Electric polarization under different H demonstrates that the magnetic field suppresses polarization. [Reproduced from Ref. 1]

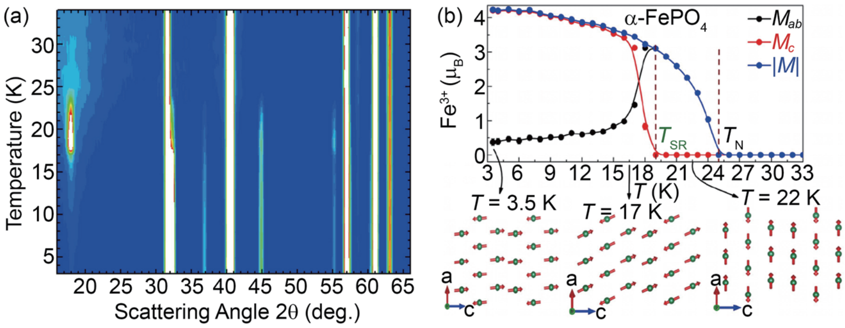

Fig. 2: (a) Temperature-dependent NPD patterns of α-FePO₄. The long-range magnetic ordering at $T_N = 25$ K and a redistribution of magnetic diffraction intensities at $T_{SR} = 17$ K. (b) The refined magnetic moment as a function of the temperature illustrates the evolution of the easy axis from the ab-plane to the c-axis. Spin structures are shown at three selected temperatures. [Reproduced from Ref. 1]

is a long-term user of ACNS and has achieved notable results in recent years. Two recent works by Yang and collaborators are highlighted in this report. The α-Iron phosphate (α-FePO₄), known as berlinite, crystallizes into a non-centrosymmetric trigonal $P3_121$ structure. In the compound, the magnetic Fe^{3+} ions form a two-dimensional layered triangular lattice on the ab-plane. Magnetic susceptibility and specific heat reveal two magnetic transitions at ~25 K and ~ 17 K, as shown in **Figs. 1(a) and 1(b)**. The reduction of magnetization below ~ 25 K indicates an antiferromagnetic order, and the second anomaly is associated with the spin reorientation transition (SR), as confirmed by the neutron diffraction experiment. The temperature dependence of dielectric constant (ε') and magnetodielectric response (MD) is shown in **Figs. 1(c) and 1(d)**. A clear correlation between the magnetic and electrical degrees of freedom is exhibited. The value of the dielectric constant is suppressed and enhanced in the temperature ranges ~17 K < T < ~25 K and T < ~17 K, respectively, manifesting the negative and positive MD effects. **Figures 1(e) and 1(f)** show the electric polarization measured in the compound. The sign of the P is flipped while reversing the polling electric field direction. The application of H significantly suppresses the electric polarization P, suggesting that P may be linked to the magnetic structure that responds to the applied magnetic field. Noticeably, the electrical polarization P exists only below ~17 K, suggesting that α-FePO₄ might be a Type-II multiferroic material, of which P is connected to the low-temperature magnetic phase.

The neutron powder diffraction (NPD) experiments were conducted on the high-intensity powder diffractometer **WOMBAT** at the Open Pool Australian Lightwater reactor (OPAL) at ANSTO. The temperature-dependent diffraction patterns are shown as a color contour in **Fig. 2(a)**. Upon cooling, new diffraction peaks of magnetic origin appear below ~24 K, and these peaks can be indexed with the magnetic wave vector k = (0, 0, 1/2), indicating that the magnetic unit cell is twice the size of the crystal structure unit cell. With further cooling, the magnetic (0, 0, -3/2) peak at 2θ ~18° reverses its trend at ~17 K, while the other peaks increase. Analysis of the NPD patterns reveals that the spin structure is collinear antiferromagnetic over the entire temperature range studied. The spins in the triangular layer are parallel, and the ferromagnetic layers are stacked alternately along the *c*-axis. The refined magnetic moment as a function of the temperature is shown in **Fig. 2(b)**. Initially, the spins lie in the ab-plane and tilt upward below ~17 K, suggesting a spin-rotation transition. Based on previous neutron studies and the present NPD analysis, the spin structure remains essentially unchanged through the transition, and α-FePO$_4$ is not a conventional Type-II multiferroic. This observation encourages further studies using Raman spectroscopy and density functional theory (DFT) calculations, leading to the conclusion that the spin-dependent p-d hybridization mechanism potentially explains the observed polarization.

Another case is the study of the polar compound VOSe$_2$O$_5$ ($P4_{CC}$).[2] This compound is a rare example of a bulk material that hosts Néel-type skyrmions. In this work, AC magnetic susceptibility measurements were performed at various temperatures, magnetic fields, and pressures, resulting in a detailed phase diagram. In the low-field regime, two magnetic transitions, labeled T_{C1} (~7.4 K) and T_{C2} (~4.0 K), are identified. The phase between T_{C2} and T_{C1} is sensitive to the magnetic field: successive phase transitions occur as the magnetic field is increased. Furthermore, a small region just below the order-disorder boundary is marked as the “A” phase in **Figs. 1(a) and 1(b)**. Remarkably, hydrostatic pressure can stabilize the skyrmion phase. The area of the skyrmion phase in the H-T phase diagram increases by approximately three times under a pressure of 14.21 kbar, as shown in **Fig. 3(b)**. Neutron diffraction is useful for characterizing these phases.

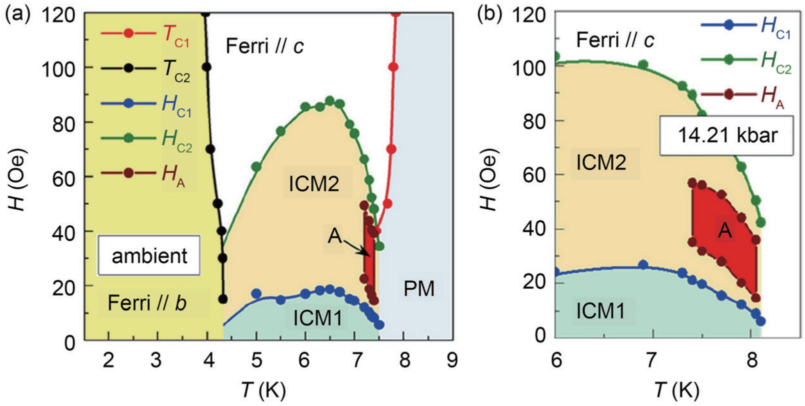

Fig. 3: *H-T* phase diagrams of VOSe$_2$O$_5$ (a) at ambient pressure and (b) under pressure P = 14.21 kbar. Both diagrams show the critical fields H_{C1} and H_{C2}, which indicate transitions between magnetic phases: ferrimagnetic (Ferri//*c*), ICM1, and ICM2. The A zone represents the skyrmion phase, and in (b), this phase expands by approximately threefold under 14.21 kbar, demonstrating that pressure effectively influences skyrmion phase stability. [Reproduced from Ref. 2]

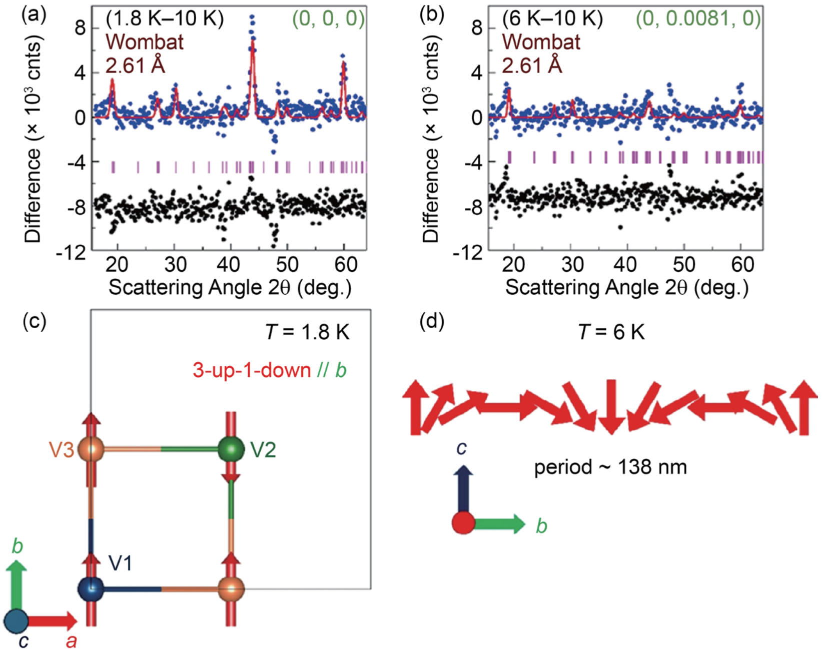

Fig. 4: (a) Neutron diffraction difference patterns between 1.8 K and 10 K highlight the pure magnetic contribution and corresponding refinement. (b) Difference patterns between 6 K and 10 K, with magnetic refinement. Purple ticks indicate magnetic reflections. The distinct temperature-dependent patterns reveal two different magnetic structures. (c,d) Illustrations of the magnetic structures at T = 1.8 K and 6 K, respectively. At 1.8 K, a three-up-one-down collinear ferrimagnetic configuration is aligned along the *b*-axis. At 6 K, an incommensurate cycloidal structure emerges, with spins rotating within the *bc*-plane and a modulation period of approximately 138 nm. This temperature-dependent evolution of the magnetic structure highlights the inherent magnetic anisotropies in this system. [Reproduced from Ref. 2]

The NPD experiments are conducted on the high-intensity powder diffractometer, **WOMBAT**. Magnetic structure determination for low-spin magnets, which may be influenced by quantum fluctuations, is generally challenging due to extremely weak magnetic signals in NPD patterns. In earlier NPD studies using a high-resolution powder diffractometer, the weak magnetic signal was not detected; however, analyzable data were obtained with the high-intensity diffractometer. **Figures 4(a) and 4(b)** present the analysis of magnetic diffraction patterns, obtained by subtracting the 10 K pattern (above T) from those collected in the ordered state. Although the data quality is not optimal, it is sufficient for comparing symmetry-constrained models.

A collinear ferrimagnetic model with spins aligned along the *b*-axis is supported by the magnetic diffraction pattern at 1.8 K. The four V^{4+} spins in the unit cell are arranged in a three-up, one-down configuration, as shown in **Fig. 4(c)**, consistent with earlier DFT results.[3] The spin structure between T_{C1} and T_{C2} that hosts a skyrmion phase is expected to be incommensurate, as indicated by various chiral compounds that exhibit skyrmion lattice phases. A recent small-angle neutron scattering (SANS) experiment reveals a magnetic propagation vector k = (0, 0.0081, 0) from a single crystal sample.[4] For such an extremely long period-modulated spin structure, the period or magnetic structure cannot be determined solely by conventional NPD. By combining the propagation vector obtained from the SANS experiment with the magnetic diffraction pattern, one can distinguish among candidate models and conclude that a cycloidal spin structure, with spins evolving in the bc-plane as illustrated in **Fig. 4(d)**, is present.

In this report, two applications of NPD in condensed matter research are summarized, demonstrating that neutron diffraction provides unique information not accessible through other experimental techniques. (Reported by Chin-Wei Wang)

*This report features the works of Hung-Duen Yang and his collaborators published in Phys. Rev. B **111**, 214418 (2025), and Phys. Rev. B **112**, 024441 (2025).*

ANSTO WOMBAT – High-Intensity Powder Diffractometer

- NPD
- Materials Science, Chemistry, Condensed-matter Physics

References

1. D. C. Kakarla, A. Tiwari, Y. H. Tseng, T. W. Yen, H. C. Wu, C. W. Wang, M.-J. Hsieh, J.-Y. Lin, A. Pal, C. Dhanasekhar, D. P. Gulo, H. L. Liu, H. D. Yang, Phys. Rev. B **111**, 214418 (2025).
2. T. W. Kuo, C. C. Chen, D. C. Kakarla, A. Tiwari, C. W. Wang, M. Gooch, L. Z. Deng, C. W. Chu, H. D. Yang, H. C. Wu, Phys. Rev. B **112**, 024441 (2025).
3. S.-H. Kim, P. S. Halasyamani, B. C. Mottot, R. Sechadri, M. A. Green, A. S. Sefat, D. Mandrus, Chem. Mater. **22**, 5074 (2010).
4. T. Kurumaji, T. Nakajima, V. Ukleev, A. Feoktystov, T. Arima, K. Kakurai, Yoshinori Tokura, Phys. Rev. Lett. **119**, 237201 (2017).

Neutron Reflectometry Probes Critical Interface Effects in Ferroelectric $Hf_{0.5}Zr_{0.5}O_2$ Films

The interfacial structure of ferroelectric $Hf_{0.5}Zr_{0.5}O_2$ thin films has been shown to strongly influence device performance.

Introducing Zr into HfO_2 thin films lowers the crystallization temperature for the ferroelectric orthorhombic phase and promotes robust ferroelectric properties. A team led by Miin-Jang Chen (National Taiwan University) and Tzu-Yen Huang (NSRRC) systematically investigated the depth-dependent structure of ferroelectric $Hf_{0.5}Zr_{0.5}O_2$ (HZO) thin films. HZO metal–ferroelectric–metal (MFM) devices with W electrodes were fabricated by atomic layer deposition using thermal (THE), plasma-assisted (PLA), and atomic layer annealing (ALA) processes, and their ferroelectric properties were evaluated.

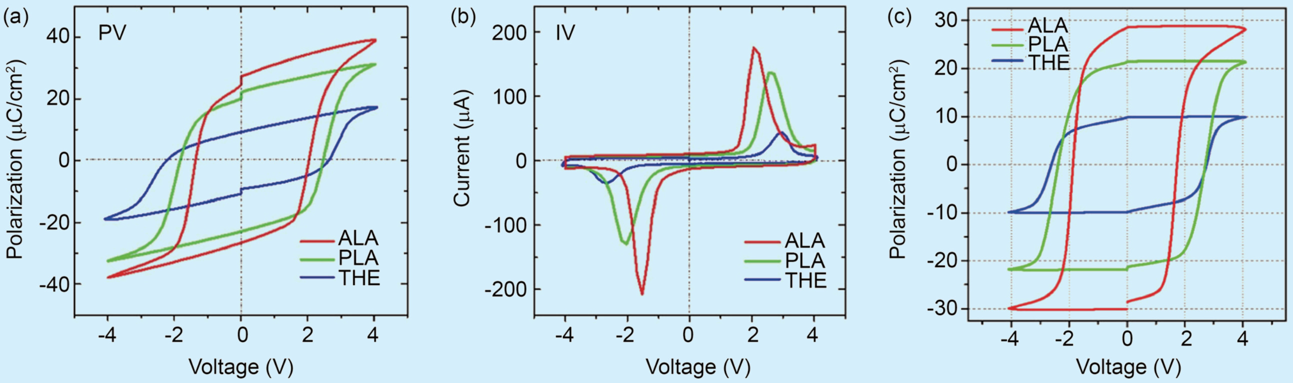

Fig. 1: (a) P–V hysteresis and (b) I–V switching responses show that the ALA device exhibits the largest Pr and the strongest switching current. (c) PUND-derived switching polarization measured with a 4 V pulse amplitude at 2 kHz confirms the most pronounced ferroelectric switching for the ALA-treated HZO film. [Reproduced from Ref. 1]

The team performed neutron reflectometry (NR) measurements on the **SPATZ** reflectometer at the Australian Nuclear Science and Technology Organisation (ANSTO) to probe buried interfaces in the HZO thin films.[1] **Figures 1(a) and 1(b)** show the polarization–voltage (P–V) hysteresis loops and current–voltage (I–V) switching characteristics of the THE, PLA, and ALA devices in the pristine state. Among these, the ALA device exhibits the largest remanent polarization (Pr) and the strongest switching current, indicating more pronounced ferroelectric switching in the ALA-processed HZO layer. **Figure 1(c)** displays the polarization switching extracted using the positive-up-negative-down (PUND) method. In this measurement, two consecutive positive pulses followed by two consecutive negative pulses are applied to isolate polarization switching while suppressing non-ferroelectric contributions, such as leakage- and capacitance-related currents, enabling a more reliable determination of 2Pr. The extracted 2Pr values are 57.9, 43.0, and 19.7 $\mu C/cm^2$ for the ALA, PLA, and THE devices, respectively. The highest 2Pr value observed for the ALA device suggests that the ALA treatment promotes a higher fraction of the ferroelectric orthorhombic phase in the HZO film, resulting in an enhanced ferroelectric response.

NR, with its high penetration depth, is well-suited for resolving the depth-dependent structure of MFM (W/HZO/W) devices and for probing buried interfaces that are challenging to access using other characterization techniques. **Figures 2(a)–2(c)** display the NR profiles for the THE, PLA, and ALA samples. The reflectivity data were analyzed using the *refnx* software,[2] where reasonable constraints were applied to the scattering length density (SLD) to ensure physically consistent refinement. The resulting fit curves show excellent agreement with the experimental data. The best-fit SLD depth profiles are summarized in **Fig. 2(d)**, highlighting distinct interfacial characteristics among the three processes.

For the THE sample, the HZO/W interfaces remain sharp, consistent with a well-defined heterointerface. The WO_X-related interfacial contributions extracted from the fits are sub-nanometer in thickness, indicating limited interdiffusion and minimal compositional grading at the HZO/W interface. By contrast, both PLA and ALA samples exhibit pronounced SLD gradients within the WO_X interfacial region, suggesting the formation of diffuse transition layers rather than an abrupt interface. Moreover, the WO_X interfacial layers in the ALA sample are thicker than those in the PLA sample. The fitted WO_X thicknesses near the top and bottom electrodes are 20 and 39 Å for the ALA sample, compared with 13 and 34 Å for the PLA sample. These results indicate stronger interfacial modification induced by the ALA treatment, potentially associated with elevated surface temperature during Ar plasma exposure. The fitted SLD values of the HZO layers are 5.5×10^{-6} Å^{-2}, 5.4×10^{-6} Å^{-2}, and 5.3×10^{-6} Å^{-2} for the ALA, PLA, and THE samples, respectively, indicating differences in film density and stoichiometry among the processes. The highest SLD observed for the ALA sample can be attributed to two factors: (1) additional Ar plasma exposure during ALA promotes film densification and improves crystallinity, and (2) the formation of a distinct WO_X interfacial layer at the bottom HZO/W interface, which can act as an oxygen reservoir during annealing. Such oxygen exchange can suppress oxygen-vacancy formation in HZO and thereby contribute to the increased SLD of the HZO layer in the ALA sample.

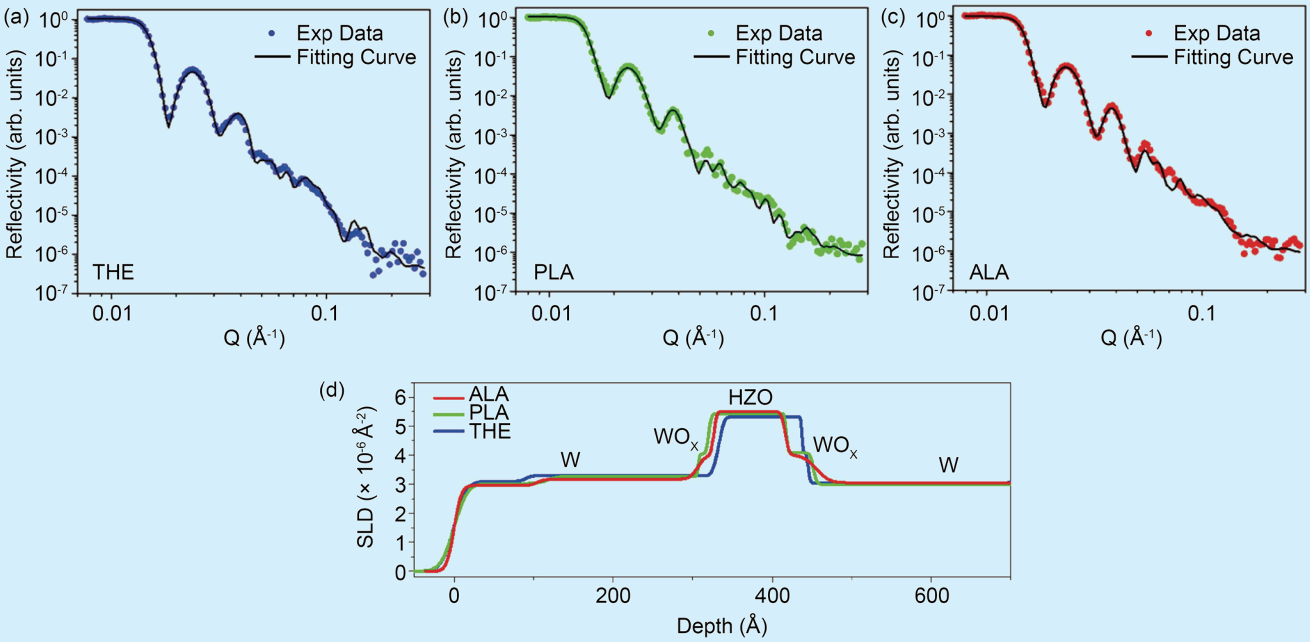

Fig. 2: NR profiles and fitting curves for HZO films prepared using (a) THE, (b) PLA, and (c) ALA methods. (d) Comparison of the corresponding SLD depth profiles extracted from reflectivity analysis. [Reproduced from Ref. 1]

In summary, this study used NR to investigate buried interfacial structures in W/HZO/W MFM devices composed of W, WO_X, and HZO layers. The NR analysis identified distinct bottom WO_X interfacial layers in the PLA and ALA samples, which can serve as oxygen reservoirs during annealing, suppressing oxygen-vacancy formation in HZO and stabilizing the ferroelectric orthorhombic phase. By contrast, the THE sample, fabricated without plasma treatment, exhibits weaker ferroelectric switching, consistent with a higher oxygen-vacancy concentration in the HZO film. Notably, the ALA treatment improves HZO densification and crystallinity and creates a more developed WO_X interfacial layer, resulting in the highest SLD and the strongest ferroelectric response. Overall, these findings provide a quantitative approach to resolving complex buried interface structures and emphasize the key role of interface engineering in enhancing HZO-based ferroelectric devices. (Reported by Tzu-Yen Huang)

This report features the work of Miin-Jang Chen and his collaborators published in ACS Appl. Mater. Interfaces ***17****, 16102 (2025).*

ANSTO SPATZ – Neutron Reflectometer
- NR
- Ferroelectric Thin Films, Atomic Layer Deposition and Interfaces

References

1. H. Y. Chen, C. L. Mo, J. J. Shyue, T. Y. Huang, M. J. Chen, ACS Appl. Mater. Interfaces **17**, 16102 (2025).
2. A. R. J. Nelson, S. W. Prescott, J. Appl. Crystallogr. **52**, 193 (2019).